

Quantum Resistor-Capacitor Circuit with Majorana Fermion Modes in Chiral Topological Superconductor

Minchul Lee¹ and Mahn-Soo Choi²

¹*Department of Applied Physics, College of Applied Science, Kyung Hee University, Yongin 446-701, Korea*

²*Department of Physics, Korea University, Seoul 136-701, Korea*

(Dated: March 26, 2014)

We investigate the mesoscopic resistor-capacitor circuit consisting of a quantum dot coupled to spatially separated Majorana fermion modes in a chiral topological superconductor. We find substantially enhanced relaxation resistance due to the nature of Majorana fermions, which are their own anti-particles and composed of particle and hole excitations in the same abundance. Further, if only a single Majorana mode is involved, the zero-frequency relaxation resistance is completely suppressed due to a destructive interference. As a result, the Majorana mode opens an exotic dissipative channel on a superconductor which is typically regarded as dissipationless due to its finite superconducting gap.

PACS numbers: 73.63.-b, 73.63.Kv, 74.90.+n, 73.43.-f

As electronic circuit is miniaturized on the nanometer scale, quantum coherence takes effect and transport properties get fundamentally different. For a ballistic conductor, Ohm's law breaks down and the conductance is quantized to multiples of $R_Q \equiv h/e^2$ [1, 2], where h is the Planck constant and e is the electron charge. For a small resistor-capacitor circuit, the charge relaxation resistance is also quantized to $R_Q/2$, irrespective of the transmission properties [3, 4], as demonstrated in an experiment on a quantum dot (QD) coupled to quantum Hall (QH) edge channel [5]. The quantization is technically ascribed to the fermi-liquid nature of the system [6–10], where the relaxation of particle-hole (p-h) pairs due to charge fluctuations at the cavity is the culprit for the dissipation. It is tempting and indeed customary [11] to interpret the quantized value as the contact resistance at a single interface (hence a half of the two-terminal contact resistance R_Q).

Here we show that when the circuit involves Majorana fermions, which are casually regarded as half-fermions, the quantum resistance defies such an interpretation. Specifically, we examine a QD coupled, with different strengths, to two *spatially separated* one-dimensional (1D) chiral Majorana fermion modes; see Fig. 1. In the ultimate limit, a single Majorana mode is considered. The primary goal is to identify the role of each Majorana mode in relaxation resistance and compare it to the case of Dirac fermion mode.

Mathematically, a Dirac fermion can always be decomposed into a pair of Majorana fermions, but these Majorana fermions usually occupy the same spatial location. However, the chiral topological superconductor (cTSC) states [12] enable physical realization of spatially separated 1D Majorana fermion modes. An example is a quantum anomalous Hall (QAH) insulator proximity-coupled to a conventional (or *normal*) superconductor (NSC) [12]. A HgTe quantum well doped with Mn element [13] and a Bi₂Te₃ thin film doped with Cr element [14, 15] turn into a QAH insulator with a chiral Dirac fermion edge mode, i.e., two chiral Majorana edge modes. When the QAH insulator is coupled to a NSC (see Fig. 1), the proximity-induced pairing potential pushes one of the two Majorana modes deeper into the bulk, spatially sep-

arating it from the other. As the relative magnitudes of the magnetization and the superconducting gap vary, the system undergoes topological phase transitions, from QAH insulator phase to a cTSC phase (hereafter called as the cTSC₂ phase) with two spatially separated Majorana edge modes [16], to another cTSC phase (called as the cTSC₁ phase) with a single Majorana edge mode (one mode having disappeared into the bulk), and finally to a NSC without any edge channel [12].

Once the system enters the cTSC phases (either cTSC₁ or cTSC₂), we find that the low-frequency relaxation resistance is no longer pinned at $R_Q/2$ and strongly depends on the transmission properties. Especially, as the QD level approaches the resonance, the zero- or finite-frequency resistance is substantially enhanced, suggesting that Majorana modes boost the p-h pair generation and are highly dissipative. It contrasts with the gapped superconductor case, in which the resistance is suppressed for frequencies ω smaller than the gap. For the cTSC₁ phase with only a single Majorana edge mode, on the other hand, we find that the low-frequency relaxation resistance vanishes in the $\omega \rightarrow 0$ limit as for the fully gapped superconductor. The vanishing resistance is attributed to the exact cancellation between p-h pair generation processes in charge-conserving and pairing channels, as will be discussed later (see Fig. 3). These exotic behaviors are distinguished from those for normal superconductors or Dirac fermion channels. This casts an intriguing question about the

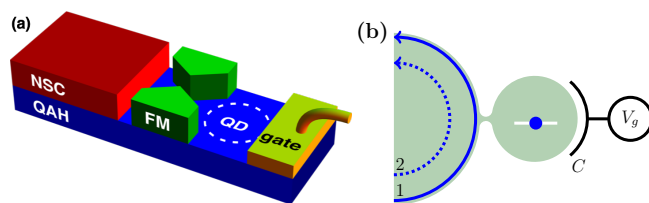


FIG. 1. (Color online) (a) A possible realization of quantum capacitor with spatially separated Majorana fermion modes. (b) A schematic of the coupling between two spatially separated Majorana edge modes ($j = 1, 2$) and the energy level localized on the QD.

role of the Majorana fermions in relaxation resistance and offers an unambiguous method to detect the Majorana fermions.

Model.— Focusing on the low-energy physics inside the bulk gap, one can describe a cTSC with two chiral Majorana modes

$$H_{\text{Majorana}} = \sum_{j=1,2} \sum_{k>0} \epsilon_k \gamma_{-k,j} \gamma_{k,j}, \quad (1)$$

where $\gamma_{k,j} = \gamma_{-k,j}^\dagger$ are chiral Majorana fermion operators, $\epsilon_k = \hbar v k$ is their energy, and v is the propagation velocity of the Majorana edge modes. In the cTSC₁ phase, we regard the mode $j = 2$ disappearing into the bulk.

The QD can be formed by depositing ferromagnetic insulators (FMs), which turns the underneath region into the trivially insulating state (I). A proper placement of FMs deforms and localizes the QAH edge states to form a QD; see Fig. 1(a). Since the localized state in the QD originates from the spin-polarized QAH edge state, it is described as a single spinless level ϵ_d :

$$H_{\text{QD}} = \{\epsilon_d + e[U(t) - V_g(t)]\} n_d. \quad (2)$$

Here $n_d = d^\dagger d$ is the occupancy operator, and the ac voltage $V_g(t)$ upon the gate coupled to the QD via a geometrical capacitance C induces the polarization charge on the dot and eventually the internal potential $U(t)$. The latter is determined self-consistently under the charge conservation condition.

The coupling of the QD level to the chiral Majorana edge modes ($j = 1, 2$) takes a tunneling model [17]

$$H_{\text{tun}} = \sum_k [t_1 d^\dagger \gamma_{k,1} + i t_2 d^\dagger \gamma_{k,2} + (\text{h.c.})]. \quad (3)$$

Here, for simplicity, we have assumed wide bands and neglected the momentum dependence of the tunneling amplitudes t_j between the Majorana mode j and the QD level. In this limit, the coupling is conveniently described by the hybridization parameters $\Gamma_j \equiv |t_j|^2 / \hbar v$ and $\Gamma_\pm \equiv (\Gamma_2 \pm \Gamma_1)/2$. In general $\Gamma_1 \geq \Gamma_2$ due to their spatially separated localizations; in particular, $\Gamma_2 = 0$ in the cTSC₁ phase and $\Gamma_1 = \Gamma_2$ only in the QAH phase. Note that our model ignores the bulk states of the reservoir and the relevant values of Γ_1 and ω should be sufficiently smaller than the bulk gap; it may be inadequate when the system is too close to the cTSC₂-cTSC₁ transition point (i.e., the bulk gap is too small).

Relaxation Resistance.— We calculate the ac current $I(t)$ between the reservoir of Majorana modes and the QD, or equivalently the displacement current between the top gate and the QD, using the self-consistent mean-field approach in the linear-response regime [3, 4, 6–10, 18, 19]. The relaxation resistance $R_q(\omega)$ is then obtained from its relation to the admittance $g(\omega)$, $1/g(\omega) = R_q(\omega) + i/\omega C_q(\omega)$, where $C_q(\omega)$ is the quantum correction to the capacitance. At zero temperature the admittance allows for a closed-form expression and

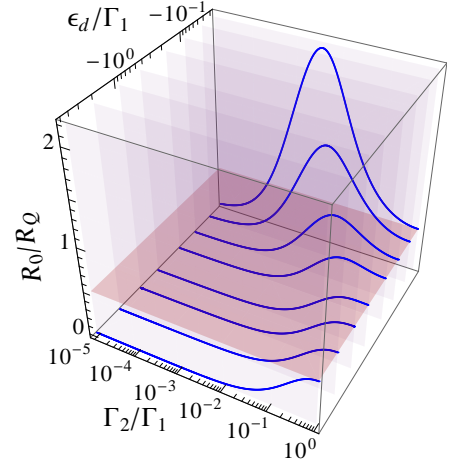


FIG. 2. (Color online) Zero-frequency relaxation resistance $R_0 = R_q(\omega \rightarrow 0)$ as a function of ϵ_d and Γ_2 . For comparison, a shaded horizontal surface is also drawn at the quantized value $R_Q/2$.

reads as (hereafter we set $\hbar = k_B = 1$)

$$g(\omega) = \frac{1}{R_Q} \sum_{\mu=\pm} \left\{ \frac{\Gamma_-^2}{\varepsilon(\omega + \mu\varepsilon)} \ln \frac{\Gamma_+ + i\varepsilon}{\Gamma_+ - i\varepsilon} + \left[\frac{\Gamma_-^2}{\varepsilon(\varepsilon + \mu\omega)} + \frac{\Gamma_+}{\Gamma_+ + i\omega} \right] \ln \frac{\Gamma_+ + i(2\omega + \mu\varepsilon)}{\Gamma_+ + i\mu\varepsilon} \right\} \quad (4)$$

with $\varepsilon \equiv \sqrt{4\epsilon_d^2 - \Gamma_-^2}$. Equation (4) is the main result of this work. We now discuss its physical implications.

Zero-frequency resistance at zero temperature.— Let us first focus on the zero-frequency limit ($\omega \ll \epsilon_d^2/\Gamma_1$) of the resistance, $R_0 \equiv R_q(\omega \rightarrow 0)$ [19]; see Fig. 2. In the QAH phase, where the two Majorana modes equally contribute ($\Gamma_1 = \Gamma_2$), the resistance restores the quantized value, $R_0 = R_Q/2$, as expected because the two Majorana modes in the QAH phase are equivalent to a single Dirac fermion mode.

As the system evolves into the cTSC₂ phase ($0 < \Gamma_2 < \Gamma_1$), R_0 does not only deviate from the quantized value but also depends on the ratio Γ_2/Γ_1 and the QD level ϵ_d , as shown in Fig. 2. When the dot level is far from the resonance ($|\epsilon_d| \gg \Gamma_1$), the zero-frequency resistance, $R_0 \approx (R_Q/2) [4(\Gamma_2/\Gamma_1)/(1 + \Gamma_2/\Gamma_1)^2]$, depends only and monotonically on the ratio Γ_2/Γ_1 ; see the curve for large values of $|\epsilon_d|$ in Fig. 2. When the dot level resonates with the Fermi level ($|\epsilon_d| \ll \Gamma_1$), it now depends non-monotonically on Γ_2/Γ_1 with the maximum at $\Gamma_2 \approx \Gamma_m \equiv 4\epsilon_d^2/\Gamma_1$ of the height $\sim [4\gamma_m \ln \gamma_m]^{-1}$ with $\gamma_m \equiv \Gamma_m/\Gamma_1$. In short, unlike the Dirac fermion case, R_0 for the reservoir of Majorana modes strongly depends on the properties of the tunneling barrier and the QD, and thus defies the simple interpretation [11] of it as a half of the two-terminal contact resistance.

The zero-frequency relaxation resistance in the cTSC₁ phase with a single Majorana mode ($\Gamma_2 = 0$) is even more interesting and exotic: it vanishes exactly, $R_0 = 0$, irrespec-

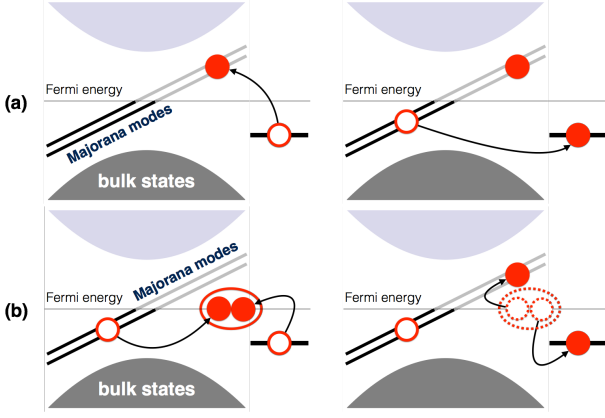


FIG. 3. (Color online) Second-order processes to generate a p-h pair in the Majorana fermion channel via (a) the charge-conserving process ($\sim |t_{\text{single}}|^2$) and (b) the pairing process ($\sim |t_{\text{pair}}|^2$) when the QD is initially occupied. The degenerate Majorana modes are artificially split here as a guide for the eye.

tive of Γ_1, Γ_2 and ϵ_d , although there is no excitation energy gap [19]. To understand it, we introduce chiral Dirac fermion operators $c_k \equiv (\gamma_{k,1} + i\gamma_{k,2})/\sqrt{2}$ composed of the two Majorana fermions, in terms of which the Hamiltonians (1) and (3), respectively, are rewritten as

$$H_{\text{Majorana}} = \sum_k \epsilon_k c_k^\dagger c_k \quad (5)$$

$$H_{\text{tun}} = \sum_k \left[t_{\text{single}} d^\dagger c_k + t_{\text{pair}} d^\dagger c_k^\dagger + (\text{h.c.}) \right] \quad (6)$$

with $t_{\text{single/pair}} \equiv (t_1 \pm t_2)/\sqrt{2}$. This form (6) immediately suggests two distinctive types of processes, as illustrated in Fig. 3: One is charge-conserving type from the t_{single} -term, in which the p-h pair is excited via the electron tunneling in and out of the QD [Fig. 3(a)]. This type of processes alone would give rise to $R_0 = R_Q/2$ [7–10]. The other is pairing type involving the t_{pair} -term which accompanies the creation and destruction of a Cooper pair in the bulk [Fig. 3(b)]. This type is missing in the QAH phase, where $t_1 = t_2$. When the QD is initially occupied, the charge-conserving (pairing) process creates the particle (hole) first. Hence the p-h pair amplitudes of the two processes are opposite in sign (at all orders) due to the fermion ordering. When $\Gamma_2 = 0$ ($t_{\text{single}} = t_{\text{pair}}$), both types are the same in magnitude so as to cancel out each other exactly. This cancellation and the subsequent vanishing resistance are hallmarks of the relaxation via the Majorana modes. Note, however, that this cancellation is exact only for $\Gamma_2 = 0$ and for p-h pairs with vanishingly small energy ($\omega \rightarrow 0$ limit). At finite ω , as shown below, the intermediate virtual states are different for two processes so that the cancellation is not perfect.

Finite-frequency resistance at zero temperature.— We find that the vanishing or enhancement of the resistance discussed above becomes even more pronounced at finite frequencies. While the finite-frequency resistance $R_q(\omega)$ is zero

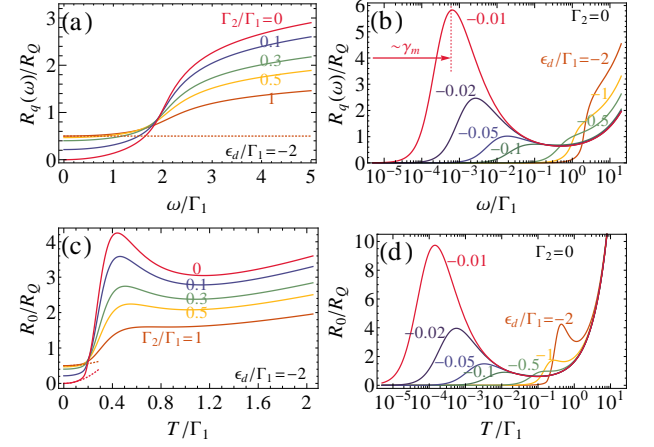


FIG. 4. (Color online) (a,b) Zero-temperature resistance $R_q(\omega) = R_q(-\omega)$ as a function of frequency ω . (c,d) Zero-frequency resistance R_0 as a function of temperature T . $\epsilon_d/\Gamma_1 = -2$ in (a,c), and $\Gamma_2 = 0$ in (b,d). The arrow in (b) indicates the approximate peak position $\sim \gamma_m$ for $\Gamma_2 = 0$ and $\epsilon_d/\Gamma_1 = -0.01$. The dotted lines in (c) correspond to the low-temperature asymptotes.

for conventional superconducting reservoir due to its finite gap, it grows with $|\omega|$ for the gapless Dirac fermion reservoir since the spectral density of p-h excitations grows with energy [7]. In the QAH phase, $R_q(\omega)$ grows slowly and monotonically with ω [Fig. 4(a)]. Entering the cTSC phase, however, $R_q(\omega)$ becomes highly non-monotonic, forming an ever narrower dip at $\omega = 0$ and peaks at $|\omega| \sim \Gamma_m$ [Fig. 4(a,b)]. The dip width is the order of Γ_m for $\Gamma_2 \approx 0$.

Let us examine the cTSC₁ phase ($\Gamma_2 = 0$) in three different regimes: the (i) off-resonance ($|\epsilon_d| \gg \Gamma_1$), (ii) near-resonance ($0 < |\epsilon_d| \ll \Gamma_1$), and (iii) exact-resonance ($\epsilon_d = 0$) regime. (i) In the off-resonance regime, the resistance grows like $R_q(\omega) \approx (R_Q/3)(\omega/\epsilon_d)^2$ for small frequencies ($\omega \ll \Gamma_m$), and keeps growing monotonically for higher frequencies. Note that in this limit the resistance is independent of the barrier transmission. (ii) In the near-resonance regime, $R_q(\omega) \approx [R_Q/3\gamma_m(\ln \gamma_m)^2](\omega/\Gamma_m)^2$ for $\omega \ll \Gamma_m$, and it shows sharp peaks at $\omega \approx \pm \Gamma_m$ [Fig. 4(b)]. The quadratic growth and dip-peak structure around $\omega = 0$ cast stark contrasts with the superconducting reservoir case. (iii) Even more dramatic contrast appears at the exact resonance. In this case, the two peaks at $\omega \approx \pm \Gamma_m$ in Fig. 4(b) merge together, filling up the dip at $\omega = 0$ (i.e., the dip width is zero). As a result, the resistance $R_q(\omega) \approx \pi R_Q/4(2|\omega|/\Gamma_1)(\ln(2|\omega|/\Gamma_1))^2$ diverges as $\omega \rightarrow 0$. In summary, the finite-frequency relaxation resistance is genuinely enhanced for $\Gamma_2 \ll \Gamma_1$ near resonance.

All-Majorana representation.— To understand the enhancement of the resistance near resonance, it is instructive to describe the dot level in terms of the language of Majorana fermions as well [19]. We define two Majorana operators $\gamma_{d,j}$ ($j = 1, 2$) by $\gamma_{d,1} = (d - d^\dagger)/\sqrt{2}i$ and $\gamma_{d,2} = (d + d^\dagger)/\sqrt{2}$. Unlike the Majorana fermions on the edge modes of the cTSC these dot Majorana fermions are rather mathematical as they occupy the same spatial location. The QD and coupling

Hamiltonians (2) and (3), respectively, read as

$$H_{\text{QD}} = i\epsilon_d \gamma_{d,2} \gamma_{d,1} \quad (7a)$$

$$H_{\text{tun}} = \sum_k i(t_2 \gamma_{d,2} \gamma_{k,2} - t_1 \gamma_{d,1} \gamma_{k,1}). \quad (7b)$$

In this expression, ϵ_d becomes the coupling between the two dot Majorana fermions. The two Majorana edge modes in the reservoir are coupled *indirectly* via the coupling between two Majorana fermions on the dot, being completely decoupled at the resonance ($\epsilon_d = 0$). However, it does not mean that their contributions are independent [see Eq. (S40) below], because the charge is always composed of two Majorana fermions. At $\epsilon_d = 0$, the real part of admittance, representing the dissipation, is expressed as

$$\text{Re}[g(\omega)] = \frac{2\pi^2}{R_Q} \omega \int_0^\omega d\omega' \rho_1(\omega - \omega') \rho_2(\omega') \quad (8)$$

where $\rho_i(\omega')$ is the density of states for $\gamma_{d,i}$, which is Lorentzian, centered at $\omega' = 0$ and with width Γ_i . If both ρ_1 and ρ_2 are finite, then $\text{Re}[g(\omega)] \sim \omega^2$ for $\omega \rightarrow 0$ so that R_0 is finite; recall $g(\omega) \approx -i\omega C_q + \omega^2 C_q^2 R_0$. However, as $\Gamma_2 \rightarrow 0$, $\rho_2(\omega')$ becomes sharper and eventually $\rho_2(\omega') = \delta(\omega')$ at $\Gamma_2 = 0$, so that $\text{Re}[g(\omega)] \sim \omega$, i.e., $R_0 \propto 1/\omega$ as seen above. In short, the resistance enhancement at resonance is attributed to a decoupled dot Majorana with abundant density of states near zero energy; the dot *electron* is coupled equally to the particle and hole components of the single Majorana edge mode so that the Majorana nature, leading to proliferation of p-h pairs, is highly pronounced.

For $\epsilon_d \neq 0$, $\gamma_{d,1}$ and $\gamma_{d,2}$ are coupled and interfere each other, causing anti-Fano-like destructive interference: The broadening of $\gamma_{d,2}$ is $\sim \Gamma_m$ and the destructive interference leads to a dip in $\rho_1(\omega)$ of width $\sim \Gamma_m$ [Fig. 4]. This is another explanation, now based on the interference between Majorana fermions, of the vanishing low-frequency resistance discussed before.

Decoherence Effects.— We remark that all the features discussed so far — the vanishing low-frequency resistance and the divergence of the resistance *at resonance* — occur only when the full coherence is maintained. In the presence of decoherence, the resistance would deviate from those coherent values. For example, when the dot is subject to random background charge fluctuations, which are the most common decoherence source on QDs, it leads to the fluctuation in ϵ_d . In effect, it pushes the system away from the resonance and the resistance does not diverge. Another indication of decoherence effects can be seen in the finite-temperature effect discussed below.

Finite-temperature effect. Typically R_q increases with temperature T since the thermal fluctuations promote the generation of p-h pairs [6]. For $T \ll \Gamma_m$, the Sommerfeld expansion [19] gives rise to $R_0 \approx R_0|_{T=0} + R_Q(2\pi^2/3)(T/\epsilon_d)^2(1 + \Gamma_-^2/\Gamma_+^2)$ in the off-resonance regime [Fig. 4(c)]: The quadratic dependence on

temperature at low temperatures suggests that the Fermi-liquid picture still works for the Majorana states. For higher temperatures, however, non-monotonic behavior is observed for $\Gamma_2 \ll \Gamma_1$ [Fig. 4(d)]: A peak occurs at $T \sim \Gamma_m$, whose height grows as $|\epsilon_d|$ decreases. The enhancement of R_q around this particular temperature is related to the peak structure in zero-temperature $R_q(\omega)$ located at $\omega \sim \Gamma_m$ as shown in Fig. 4(b). In the presence of thermal fluctuations, the contribution of low-energy p-h pairs that are suppressed due to the destructive interference between $\gamma_{d,1}$ and $\gamma_{d,2}$ decreases. Instead the p-h pairs, which have energy $\sim \Gamma_m$ and are not affected by the cancellation, cause the surge of the resistance. Together with the non-monotonic frequency dependence of $R_q(\omega)$, the peak structure driven by the thermal excitations are unique features of dissipation via Majorana states.

Acknowledgments. This work was supported by the NRF grants funded by the Korea government (MSIP) (Nos. 2011-0030046 and 2011-0012494).

-
- [1] B. J. van Wees, H. van Houten, C. W. J. Beenakker, J. G. Williamson, L. P. Kouwenhoven, D. van der Marel, and C. T. Foxon, *Phys. Rev. Lett.* **60**, 848 (1988).
 - [2] D. A. Wharam, T. J. Thornton, R. Newbury, M. Pepper, H. Ahmed, J. E. F. Frost, D. G. Hasko, D. C. Peacock, D. A. Ritchie, and G. A. C. Jones, *J. Phys. Chem.* **21**, L209 (1988).
 - [3] M. Büttiker, H. Thomas, and A. Prêtre, *Phys. Lett. A* **180**, 364 (1993).
 - [4] M. Büttiker, A. Prêtre, and H. Thomas, *Phys. Rev. Lett.* **70**, 4114 (1993).
 - [5] J. Gabelli, G. Fève, J.-M. Berroir, B. Plaçais, A. Cavanna, B. Etienne, Y. Jin, and D. C. Glatli, *Science* **313**, 499 (2006).
 - [6] S. Nigg, R. López, and M. Büttiker, *Phys. Rev. Lett.* **97**, 206804 (2006).
 - [7] M. Lee, R. López, M.-S. Choi, T. Jonckheere, and T. Martin, *Phys. Rev. B* **83**, 201304 (2011).
 - [8] C. Mora and K. Le Hur, *Nature Phys.* **6**, 697 (2010).
 - [9] M. Filippone, K. Le Hur, and C. Mora, *Phys. Rev. Lett.* **107**, 176601 (2011).
 - [10] H. Khim, S.-Y. Hwang, and M. Lee, *Phys. Rev. B* **87**, 115312 (2013).
 - [11] M. Büttiker, *J. Korean Phys. Soc.* **34**, 121 (1999).
 - [12] X.-L. Qi, T. L. Hughes, and S.-C. Zhang, *Phys. Rev. B* **82**, 184516 (2010).
 - [13] C.-X. Liu, X.-L. Qi, X. Dai, Z. Fang, and S.-C. Zhang, *Phys. Rev. Lett.* **101**, 146802 (2008).
 - [14] R. Yu, W. Zhang, H.-J. Zhang, S.-C. Zhang, X. Dai, and Z. Fang, *Science* **329**, 61 (2010).
 - [15] C.-Z. Chang, J. Zhang, X. Feng, J. Shen, Z. Zhang, M. Guo, K. Li, Y. Ou, P. Wei, L.-L. Wang, Z.-Q. Ji, Y. Feng, S. Ji, X. Chen, J. Jia, X. Dai, Z. Fang, S.-C. Zhang, K. He, Y. Wang, L. Lu, X.-C. Ma, and Q.-K. Xue, *Science* **340**, 167 (2013).
 - [16] (), to be precise, the QAH and cTSC₂ phase are *topologically* indistinguishable. Here we distinguish them for convenience in discussions of various limits.
 - [17] R. Žitko, *Phys. Rev. B* **83**, 195137 (2011).
 - [18] A.-P. Jauho, N. Wingreen, and Y. Meir, *Phys. Rev. B* **50**, 5528 (1994).

- [19] (), see the Supplementary Materials for detailed explanation of methods and expressions.
- [20] N. Wingreen, A.-P. Jauho, and Y. Meir, *Phys. Rev. B* **48**, 8487 (1993).
- [21] A. F. Andreev, *Sov. Phys. JETP* **22**, 455 (1966).
- [22] A. V. Shytov, P. A. Lee, and L. S. Levitov, *Physics-Uspekhi* **41**, 207 (1998).
- [23] A. F. Volkov, P. H. C. Magnée, B. J. van Wees, and T. M. Klapwijk, *Physica C* **242**, 261 (1995).
- [24] N. Read and D. Green, *Phys. Rev. B* **61**, 10267 (2000).
- [25] M. Sato and S. Fujimoto, *Phys. Rev. B* **79**, 094504 (2009).
- [26] P. G. de Gennes, *Superconductivity of Metals and Alloys* (Westview Press, New York, 1999).

Supplementary Materials

MODEL HAMILTONIANS

The Hamiltonian for the Majorana edge modes is constructed based on that of the Dirac fermion edge mode as given in Eq. (6) in the main text. In the absence of superconductivity, the Hamiltonian (6) is that for the QAH edge mode. Via the relation $c_k = (\gamma_{k,1} + i\gamma_{k,2})/2$, or inversely

$$\gamma_{k,1} = \frac{c_k + c_{-k}^\dagger}{\sqrt{2}} \quad \text{and} \quad \gamma_{k,2} = \frac{c_k - c_{-k}^\dagger}{\sqrt{2}i}, \quad (\text{S9})$$

the Dirac fermion Hamiltonian (6) turns into the Majorana fermion Hamiltonian (1). Proximity-coupled to a s -wave superconductor, two Majorana fermion modes are spatially separated. However, they are still degenerate in energy [12]. Therefore, the Hamiltonians (6) and (7) are valid in the cTSC₂ phase. In the cTSC₁ phase, the $j = 2$ Majorana mode becomes gapped so that it is missing. In our study, the disappearance of $j = 2$ mode is accounted for by turning off its coupling to the dot: $t_2 = 0$, see below.

The build-up of the tunneling Hamiltonian between the Majorana fermion modes and the dot electron starts with the fermionic coupling Hamiltonian which couples the QAH edge modes and the dot electron:

$$H_{\text{tun}}^{\text{QAH}} = \sum_k [t_k d^\dagger c_k + (\text{h.c.})], \quad (\text{S10})$$

where t_k is the momentum-dependent tunneling amplitude. In terms of the MF operators, it reads

$$H_{\text{tun}}^{\text{QAH}} = \sum_k \frac{1}{\sqrt{2}} [t_k d^\dagger \gamma_{k,1} + it_k d^\dagger \gamma_{k,2} + (\text{h.c.})]. \quad (\text{S11})$$

Upon the proximity-induced superconductivity, the overlaps between the Majorana modes and the dot electron become different for $j = 1, 2$ due to the different spatial localization of the Majorana modes [12]. So t_k now has the j -dependence, $t_{k,j}$ [17] so that one obtains the tunneling Hamiltonian (3) with $|t_{1,k}| > |t_{2,k}|$. In terms of the Dirac fermion operator and dropping the k -dependence, the tunneling Hamiltonian is rewritten as Eq. (7), in which the pairing term, missing in the original QAH edge Hamiltonian, appears. Hence the pairing term, whose amplitude is $t_{\text{pair}} = (t_1 - t_2)/\sqrt{2}$, is due to the mismatch in the coupling of the dot electron to two Majorana modes.

LINEAR-RESPONSE ADMITTANCE AND RELAXATION RESISTANCE

Self-consistent Linear-Response Theory

We consider a nanoscale capacitor (quantum dot) coupled to the Majorana fermion reservoir. A weak time-dependent external gate voltage $V_g(t) = V_{\text{ac}} \cos \omega t$ is applied on the quantum dot. In such a coherent RC circuit, the AC transport is highly sensitive to the internal distribution of charges and potentials, which needs to be calculated in a self-consistently manner to ensure the gauge invariance and current conservation [3, 4, 6, 7, 10]. In the mean-field approximation, the time-dependent voltage $V_g(t)$ induces the polarization charges $N_U(t)$ between the dot and the gate, which in turn leads to the time-dependent potential $U(t) = |e|N_U(t)/C$ inside the dot. Consequently, the applied voltage not only generates a current $I(t)$ between the lead and the dot, but also induces a dot-gate displacement current $I_d(t) = e(dN_U/dt) = -C(dU/dt)$. Charge conservation

requires $I(t) + I_d(t) = 0$. Assuming that the gate-invariant perturbation, $V_g(t) - U(t)$, is sufficiently small, the linear response theory leads to the relation, $I(\omega) = g(\omega)(V_g(\omega) - U(\omega))$, where $g(t) = (ie/\hbar) \langle [I(t), n_d] \rangle \Theta(t)$ is the equilibrium correlation function between the occupation operator $n_d = d^\dagger d$ and the current operator $I = e(dn_d/dt)$. Note that the current-density correlation function $g(\omega)$ is directly related to the charge susceptibility $\chi_c(t) = -i \langle [n_d(t), n_d] \rangle \Theta(t)$, via the relation $g(\omega) = i\omega(e^2/\hbar)\chi_c(\omega)$. Then, with the help of $I(\omega) = -I_d(\omega) = -i\omega C U(\omega)$, the dot-lead impedance $Z(\omega) = V_g(\omega)/I(\omega)$, which is experimentally accessible, is given by $Z(\omega) = 1/(-i\omega C) + 1/g(\omega)$. Then, the relaxation resistance and the quantum correction to the capacitance is obtained by $1/g(\omega) = R_q(\omega) + i/\omega C_q(\omega)$. Explicitly, the relaxation resistance is given by

$$R_q(\omega) = \text{Re} \left[\frac{1}{g(\omega)} \right] = \frac{\text{Re}[g(\omega)]}{\text{Re}[g(\omega)]^2 + \text{Im}[g(\omega)]^2}. \quad (\text{S12})$$

In the low-frequency limit, usually $|\text{Re}[g(\omega)]| \ll |\text{Im}[g(\omega)]|$ (since $\text{Im}[g(\omega)] \propto \omega$ and $\text{Re}[g(\omega)] \propto \omega^2$) so that

$$R_q(\omega) \approx \frac{\text{Re}[g(\omega)]}{\text{Im}[g(\omega)]^2}, \quad (\text{S13})$$

which means that the low-frequency relaxation resistance is proportional to the real part of the admittance. Accordingly, we have examined $\text{Re}[g(\omega)]$ in the main text in order to estimate the amplitude of the dissipation.

Green's Function and Admittance

While the admittance can be obtained in terms of the charge susceptibility, we instead follow the Wingreen-Meir formalism [18, 20] which derives directly the current formula for arbitrary gauge-invariant perturbation $V_g(t) - U(t)$ and then obtains the admittance by considering the linear response only. Before following the formalism, it is convenient to apply a gauge transformation which transfers the time-dependence from the QD Hamiltonian to the tunneling Hamiltonian. Under the time-dependent unitary transformation $U = \exp[\frac{i}{\hbar} S(t)]$ defined as

$$S(t) = \int^t dt' e(U(t') - V_g(t')) n_d, \quad (\text{S14})$$

the Hamiltonian is transformed into

$$H = H_{\text{Majorana}} + H_{\text{QD}} + H_{\text{tun}}(t). \quad (\text{S15})$$

Here H_{Majorana} is unchanged, $H_{\text{QD}} = \epsilon_d n_d$, and

$$H_{\text{tun}} = \sum_k [t_1(t) d^\dagger \gamma_{k,1} + i t_2(t) d^\dagger \gamma_{k,2} + (\text{h.c.})] \quad (\text{S16})$$

with $t_j(t) = t_j e^{i\Delta(t)}$ and

$$\Delta(t) \equiv \frac{i}{\hbar} \int^t dt' e(U(t') - V_g(t')). \quad (\text{S17})$$

Based on the gauge-transformed Hamiltonian, it is quite straightforward to setup non-equilibrium Green's functions and Dyson equations for them. Since the Majorana fermion comes from the superconductivity, it is useful to express the Green's function in Nambu space. The retarded/advanced/lesser QD Green's functions are then written as

$$G_d^{R/A}(t, t') = \mp i \Theta(\pm(t - t')) \begin{bmatrix} \langle |\{d(t), d^\dagger(t')\}| \rangle & \langle |\{d(t), d(t')\}| \rangle \\ \langle |\{d^\dagger(t), d^\dagger(t')\}| \rangle & \langle |\{d^\dagger(t), d(t')\}| \rangle \end{bmatrix} \quad (\text{S18a})$$

$$G_d^<(t, t') = i \begin{bmatrix} \langle |d^\dagger(t') d(t)| \rangle & \langle |d(t') d(t)| \rangle \\ \langle |d^\dagger(t') d^\dagger(t)| \rangle & \langle |d(t') d^\dagger(t)| \rangle \end{bmatrix} \quad (\text{S18b})$$

and their Dyson's equations are found to be

$$G_d^{R/A}(t, t') = g_d^{R/A}(t - t') + \int dt'' \int dt''' g_d^{R/A}(t - t'') \Sigma^{R/A}(t'', t''') G_d^{R/A}(t''', t') \quad (\text{S19a})$$

$$G_d^<(t, t') = \int dt'' \int dt''' G_d^R(t, t'') \Sigma^<(t'', t''') G_d^A(t''', t'). \quad (\text{S19b})$$

Here $\Sigma^{R/A/<}(t, t')$ are the self energies defined as

$$\Sigma^{R/A/<}(t, t') \equiv \sum_k \frac{M^\dagger(t)}{\hbar} g_k^{R/A/<}(t - t') \frac{M(t')}{\hbar}. \quad (\text{S20})$$

The QD-Majorana coupling matrix $M(t)$ in the Nambu space is given by

$$M(t) \equiv \begin{bmatrix} t_{\text{single}}^* & -t_{\text{pair}} \\ t_{\text{pair}}^* & -t_{\text{single}} \end{bmatrix} e^{-i\Delta(t)\sigma_3} \quad (\text{S21})$$

and $g_d^{R/A/<}(t)$ and $g_k^{R/A/<}(t)$ are unperturbed equilibrium retarded/advanced/lesser QD and Dirac fermion Green's functions which are expressed in the frequency domain as

$$g_d^{R/A}(\omega') = \frac{1}{\omega' - \sigma_3 \epsilon_d / \hbar \pm i0^+}, \quad g_d^<(\omega') = 2\pi f(\hbar\omega') \delta(\omega' - \sigma_3 \epsilon_d / \hbar), \quad (\text{S22a})$$

$$g_k^{R/A}(\omega') = \frac{1}{\omega' - \sigma_3 \epsilon_k / \hbar \pm i0^+}, \quad g_k^<(\omega') = 2\pi f(\hbar\omega') \delta(\omega' - \sigma_3 \epsilon_k / \hbar), \quad (\text{S22b})$$

respectively. Here $f(\epsilon)$ is the Fermi distribution function at temperature T . In the absence of the AC driving ($\Delta(t) = 0$), the Dyson's equations lead to the equilibrium QD Green's functions

$$G_d^{R/A}(\omega') = \left[g_d^{R/A}(\omega') - \Sigma^{R/A}(\omega') \right]^{-1} \quad \text{and} \quad G_d^<(\omega') = G_d^R(\omega') \Sigma^<(\omega') G_d^A(\omega') \quad (\text{S23})$$

with the equilibrium self energies given by

$$\Sigma^{R/A}(\omega') = \mp \frac{i}{2} \begin{bmatrix} \Gamma_+ & \Gamma_- \\ \Gamma_- & \Gamma_+ \end{bmatrix} \quad \text{and} \quad \Sigma^<(\omega') = i f(\hbar\omega') \begin{bmatrix} \Gamma_+ & \Gamma_- \\ \Gamma_- & \Gamma_+ \end{bmatrix}, \quad (\text{S24})$$

where Γ_\pm is as defined in the main text. The explicit form of the equilibrium retarded/advanced Green's functions in Eq. (S23) are given by

$$G_d^{R/A}(\omega) = \left[\begin{array}{cc} \omega - \epsilon_d \pm i \frac{\Gamma_\pm}{2} & \pm i \frac{\Gamma_-}{2} \\ \pm i \frac{\Gamma_-}{2} & \omega + \epsilon_d \pm i \frac{\Gamma_\pm}{2} \end{array} \right]^{-1}. \quad (\text{S25})$$

In the presence of small AC driving, suppose that $V_g(t) - U(t) \equiv V_{\text{ac}} \cos \omega t$ and accordingly,

$$\Delta(t) = -\frac{eV_{\text{ac}}}{\hbar\omega} \sin \omega t \equiv v \sin \omega t. \quad (\text{S26})$$

Up to the linear order in v , the non-equilibrium QD Green's functions are expanded as

$$\begin{aligned} G_d^{R/A}(\omega', \omega'') &= \frac{1}{2\pi} \int dt' \int dt'' e^{i(\omega't' - \omega''t'')} G_d^{R/A}(t', t'') \\ &= G_d^{R/A}(\omega') \delta(\omega' - \omega'') + \frac{v}{2} \left((1 + \omega G_d^{R/A}(\omega')) \sigma_3 G_d^{R/A}(\omega' + \omega) - G_d^{R/A}(\omega') \sigma_3 \right) \delta(\omega' - \omega'' + \omega) \\ &\quad - \frac{v}{2} \left((1 - \omega G_d^{R/A}(\omega')) \sigma_3 G_d^{R/A}(\omega' - \omega) - G_d^{R/A}(\omega') \sigma_3 \right) \delta(\omega' - \omega'' - \omega) \end{aligned} \quad (\text{S27a})$$

$$\begin{aligned} G_d^<(t, t') &= \int \frac{d\omega'}{2\pi} e^{i\omega'(t'-t)} \left[G_d^R(\omega') \Sigma^<(\omega') G_d^A(\omega') \right. \\ &\quad + \frac{v}{2} \left(e^{+i\omega t} (1 + \omega G_d^R(\omega' - \omega)) - e^{-i\omega t} (1 - \omega G_d^R(\omega' + \omega)) \right) \sigma_3 G_d^R(\omega') \Sigma^<(\omega') G_d^A(\omega') \\ &\quad \left. + \frac{v}{2} G_d^R(\omega') \Sigma^<(\omega') G_d^A(\omega') \sigma_3 \left(e^{-i\omega t'} (1 + \omega G_d^A(\omega' - \omega)) - e^{+i\omega t'} (1 - \omega G_d^A(\omega' + \omega)) \right) \right]. \end{aligned} \quad (\text{S27b})$$

For later use, we also need to define the QD-Dirac fermion Green's functions $G_{d,k}^{< / > / t / \bar{t}}$ similarly to the QD Green's functions: For example,

$$G_{d,k}^<(t, t') = i \begin{bmatrix} \langle |c_k^\dagger(t') d(t)| \rangle & \langle |c_k(t') d(t)| \rangle \\ \langle |c_k^\dagger(t') d^\dagger(t)| \rangle & \langle |c_k(t') d^\dagger(t)| \rangle \end{bmatrix} \quad \text{and} \quad G_{d,k}^t(t, t') = -i \begin{bmatrix} \langle |\mathcal{T}_c d(t) c_k^\dagger(t')| \rangle & \langle |\mathcal{T}_c d(t) c_k(t')| \rangle \\ \langle |\mathcal{T}_c d^\dagger(t) c_k^\dagger(t')| \rangle & \langle |\mathcal{T}_c d^\dagger(t) c_k(t')| \rangle \end{bmatrix}. \quad (\text{S28})$$

The equation-of-motion method relates the QD-Dirac fermion Green's functions to the QD Green's functions via the following Dyson's equations:

$$\widehat{G}_{d,k}(t, t') = \int dt'' \widehat{G}_d(t, t'') \frac{M^\dagger(t'')}{\hbar} \tau_3 \widehat{g}_k(t'', t'), \quad (\text{S29})$$

where \widehat{g}_k , \widehat{G}_d and so on are the matrix forms of the Green's functions such as

$$\widehat{g}_k \equiv \begin{bmatrix} g_k^t & g_k^{<} \\ g_k^{>} & g_k^t \end{bmatrix} \quad \text{and} \quad \widehat{G}_d \equiv \begin{bmatrix} G_d^t & G_d^{<} \\ G_d^{>} & G_d^t \end{bmatrix} \quad (\text{S30})$$

and τ_3 are the Pauli matrix in the Keldysh space.

Now we are ready to express the current $I(t)$ in terms of the QD Green's functions. The current, being the expectation value of the current operator $e(dn_d/dt)$, is expressed as

$$I(t) = e \left\langle \frac{dn_d}{dt} \right\rangle = \frac{ie}{\hbar} \sum_k \left[t_{\text{single}}^*(t) \langle |c_k^\dagger(t) d(t)| \rangle + t_{\text{pair}}^*(t) \langle |c_k(t) d(t)| \rangle - (\text{h.c.}) \right] = \frac{2e}{\hbar} \text{Re} \sum_k \left[G_{d,k}^{<}(t) M(t) \right]_{11}. \quad (\text{S31})$$

Using the Dyson's equation, Eq. (S29), the current can be written solely in terms of the QD Green's function:

$$I(t) = 2e \text{Re} \int dt' \left[G_d^R(t, t') \Sigma^{<}(t', t) + G_d^{<}(t, t') \Sigma^A(t', t) \right]_{11}. \quad (\text{S32})$$

By substituting the linearized QD Green's functions, Eq. (S27) into the current formula and performing a tedious arrangement, the linear-response current with respect to the AC signal with frequency ω , Eq. (S26) is obtained by

$$I(\omega) = \frac{e v \omega^2}{2\pi} \int d\omega' f(\hbar\omega') \left[G_d^R(\omega' - \omega) \sigma_3 (G_d^R(\omega') - G_d^A(\omega')) + (G_d^R(\omega') - G_d^A(\omega')) \sigma_3 G_d^A(\omega' + \omega) \right]_{11}. \quad (\text{S33})$$

In obtaining the above formula one has to use the following relations in equilibrium:

$$\begin{aligned} G_d^R(\omega) \Sigma^{<}(\omega) G_d^A(\omega) &= f(\hbar\omega) (G_d^A(\omega) - G_d^R(\omega)), \quad \Sigma^{<}(\omega) = -f(\epsilon) (\Sigma^R(\omega) - \Sigma^A(\omega)), \\ \text{and} \quad g_d^{-1} G_d^{R/A} - \Sigma^{R/A} G_d^{R/A} &= G_d^{R/A} g_d^{-1} - G_d^{R/A} \Sigma^{R/A} = 1. \end{aligned} \quad (\text{S34})$$

Hence we arrive at the admittance $g(\omega) = I(\omega)/V_{\text{ac}}$ given by

$$g(\omega) = \frac{\omega}{R_Q} \int d\omega' f(\omega') \left[G_d^R(\omega' - \omega) \sigma_3 \{ G_d^R(\omega') - G_d^A(\omega') \} + \{ G_d^R(\omega') - G_d^A(\omega') \} \sigma_3 G_d^A(\omega' + \omega) \right]_{11}. \quad (\text{S35})$$

Relaxation Resistance at Zero Temperature

While the finite-temperature admittance is numerically calculated by directly using Eq. (S35), the zero-temperature admittance allows the closed-form expression as given in Eq. (4) in the main text, by using the integral

$$\int_{-\infty}^0 \frac{dx}{x + a + ib} = \ln \frac{|b| - i(\text{sgn } b)a}{|b| - i(\text{sgn } b)(-\infty)}. \quad (\text{S36})$$

The zero-frequency relaxation resistance can be obtained by taking the $\omega \rightarrow 0$ limit:

$$R_0 = \frac{R_Q}{2} \frac{\Gamma_1 \Gamma_2}{\Gamma_+^2} \left(\frac{(\varepsilon/2)^2}{(\epsilon_d/\hbar)^2 - ((2\epsilon_d/\hbar)^2 + \Gamma_1 \Gamma_2) \Gamma_c / 8\Gamma_+} \right)^2 \quad (\text{S37})$$

with

$$\Gamma_c \equiv \frac{i\Gamma_-^2}{\varepsilon} \ln \frac{\Gamma_+ - i\varepsilon}{\Gamma_+ + i\varepsilon} \quad \text{and} \quad \varepsilon \equiv \sqrt{(2\epsilon_d/\hbar)^2 - \Gamma_-^2}. \quad (\text{S38})$$

Note that Γ_c is always real. The weak-coupling value of the resistance, Eq. (5) can be readily obtained by taking the limit $|\epsilon_d/\hbar| \gg \Gamma_1$ in Eq. (S37).

Two important features of the zero-frequency resistance should be remarked here. First, the zero-frequency resistance, Eq. (S37) vanishes exactly, $R_0 = 0$ if the $j = 2$ Majorana mode is detached ($\Gamma_2 = 0$), irrespective of the QD level and the transmission of the tunneling barrier. Second, near the resonance ($|\epsilon_d| \ll \Gamma_1$), R_0 , as a function of Γ_2 , has a local maximum in the interval $0 < \Gamma_2 < \Gamma_1$. The maximum occurs at $\Gamma_2 \approx \Gamma_m \equiv 4\epsilon_d^2/\Gamma_1$, and its height scales as $\sim [4\gamma_m \ln \gamma_m]^{-1}$ with $\gamma_m \equiv \Gamma_m/\Gamma_1$. Hence, as the resonance comes closer, the maximum of the resistance diverges.

Now consider the finite-frequency resistance in the cTSC₁ phase ($\Gamma_2 = 0$). Since $R_0 = 0$ in this phase, the leading-order term of the low-frequency resistance with respect to the frequency should be of the second order in ω . Explicitly,

$$R_q(\omega) = \frac{R_Q}{3} \left(\frac{(\epsilon_d/\hbar)^2 - (\Gamma_1/4)^2}{(\epsilon_d/\hbar)^3 \left(1 - \frac{\Gamma_1}{4} \frac{i}{\varepsilon} \ln \frac{\Gamma_1/2 - i\varepsilon}{\Gamma_1/2 + i\varepsilon} \right)} \right)^2 \omega^2 + \mathcal{O}(\omega^4). \quad (\text{S39})$$

Equations (8) and (9) in the main text can be obtained by taking the limits $|\epsilon_d/\hbar| \gg \Gamma_1$ and $|\epsilon_d/\hbar| \ll \Gamma_1$, respectively.

Interesting finite-frequency behavior arises at the resonance ($\epsilon_d = 0$). In this condition, the $j = 1$ and $j = 2$ Majorana modes 1 and 2 are completely decoupled as discussed in the main text and below. However, two modes still interfere with each other in the electron transport, as can be seen in the expression of the admittance:

$$g(\omega) = \frac{-i\omega}{R_Q} \left(\frac{\Gamma_1}{\omega^2 - i\Gamma_2\omega - \Gamma_+\Gamma_-} \ln \frac{\Gamma_2 + i(2\omega)}{\Gamma_2} + \frac{\Gamma_2}{\omega^2 - i\Gamma_1\omega + \Gamma_+\Gamma_-} \ln \frac{\Gamma_1 + i(2\omega)}{\Gamma_1} - \frac{2\Gamma_-}{\Gamma_-^2 + \omega^2} \ln \frac{\Gamma_2}{\Gamma_1} \right). \quad (\text{S40})$$

In the cTSC₁ phase, the finite-frequency resistance is then obtained by setting $\Gamma_2 = 0$ so that

$$R_q(\omega) = R_Q \frac{\omega^2 + (\Gamma_1/2)^2}{\Gamma_1|\omega|} \frac{\pi/2}{(\pi/2)^2 + (\ln(2|\omega|/\Gamma_1))^2} \quad (\text{S41})$$

which is approximated as Eq. (10) in the $\omega \rightarrow 0$ limit. Therefore, it exhibits a divergence at zero frequency.

All-Majorana Representation

As proposed in the main text, all the fermion operators in the Hamiltonian, including the QD electron operator, can be, at least mathematically, decomposed into the Majorana fermion operators. Defining two QD Majorana operators $\gamma_{d,j}$ ($j = 1, 2$) by $\gamma_{d,1} = (d - d^\dagger)/\sqrt{2}i$ and $\gamma_{d,2} = (d + d^\dagger)/\sqrt{2}$, the QD and tunneling Hamiltonians are rewritten as

$$H_{\text{QD}} = i(\epsilon_d + e(U(t) - V_g(t))\gamma_{d,2}\gamma_{d,1} \quad (\text{S42a})$$

$$H_{\text{tun}} = \sum_k i(t_2\gamma_{d,2}\gamma_{k,2} - t_1\gamma_{d,1}\gamma_{k,1}), \quad (\text{S42b})$$

respectively. These equations become Eq. (11) in the main text in the DC limit ($V_g(t) = U(t) = 0$). In deriving the above Hamiltonians, we assume that the tunneling amplitudes are real: $t_j = t_j^*$, which can be always satisfied via a proper gauge transformation. Applying the time-dependent unitary transformation $U = \exp[\frac{i}{\hbar}S(t)]$ as defined in Eq. (S14), the time-dependence moves into the tunneling Hamiltonian so that we have

$$H_{\text{QD}} = i\epsilon_d\gamma_{d,2}\gamma_{d,1} \quad (\text{S43a})$$

$$H_{\text{tun}} = \sum_k i[-t_1 \cos \Delta(t)\gamma_{d,1}\gamma_{k,1} + t_1 \sin \Delta(t)\gamma_{d,2}\gamma_{k,1} + t_2 \sin \Delta(t)\gamma_{d,1}\gamma_{k,2} + t_2 \cos \Delta(t)\gamma_{d,2}\gamma_{k,2}]. \quad (\text{S43b})$$

It should be noted that in the DC limit the $j = 1$ and $j = 2$ Majorana modes are completely decoupled at the resonant condition ($\epsilon_d = 0$). However, the gauge-transformed Hamiltonian (S43) shows that a finite ac driving effectively couples the $j = 1$ and $j = 2$ Majorana modes even if the dot level is zero ($\epsilon_d = 0$). This is the reason why the two Majorana modes interfere with each other in the electron transport even at resonance (see Eq. (S40)).

Now we follow the procedure of the linear-response theory as done in Sec. 2B by redefining the QD Green's function in terms of the Majorana fermion operators:

$$G_{d,M}^{R/A}(t, t') = \mp i\Theta(\pm(t - t')) \left[\langle |\{\gamma_{d,1}(t), \gamma_{d,1}(t')\}| \rangle \langle |\{\gamma_{d,1}(t), \gamma_{d,2}(t')\}| \rangle \right] \quad (\text{S44})$$

In fact, the forms of the Dyson's equations for Majorana Green's functions are identical to those in Sec. 2B except that all the Green's functions are properly replaced by the Majorana-based ones. Finally we then obtain the admittance

$$g(\omega) = \frac{\omega}{R_Q} \int d\omega' f(\omega') \text{tr} \left[(G_{d,M}^R(\omega' - \omega) \sigma_2 \{G_{d,M}^R(\omega') - G_{d,M}^A(\omega')\} + \{G_{d,M}^R(\omega') - G_{d,M}^A(\omega')\} \sigma_2 G_{d,M}^A(\omega' + \omega)) \frac{\sigma_0 + \sigma_2}{2} \right]. \quad (\text{S45})$$

Here the appearance of additional Pauli matrices is owing to the unitary transformation from the QD fermion operator to the Majorana fermion operator. The equilibrium retarded/advanced QD Green's functions are given by

$$G_{d,M}^{R/A} = \left([g_{d,M}^{R/A}(\omega)]^{-1} - \Sigma^{R/A}(\omega) \right)^{-1} = \begin{bmatrix} \omega \pm i \frac{\Gamma_1}{2} & -i\epsilon_d/\hbar \\ i\epsilon_d/\hbar & \omega \pm i \frac{\Gamma_2}{2} \end{bmatrix}^{-1}. \quad (\text{S46})$$

The Green's functions, whose off-diagonal components vanish at $\epsilon_d = 0$, reflect that the two modes are decoupled at resonance. The real and imaginary parts of the diagonal components of the Green's functions can be expressed in terms of the density of states $\rho_j(\omega)$ in such a way that

$$\text{Im}[G_{d,M}^R]_{jj}(\omega) = -\pi\hbar\rho_j(\omega) \quad (\text{S47a})$$

$$\text{Re}[G_{d,M}^R]_{jj}(\omega) = \frac{1}{\pi} \mathcal{P} \int d\omega' \frac{\text{Im}[G_{d,M}^R]_{jj}(\omega')}{\omega' - \omega} = -\mathcal{P} \int d\epsilon' \frac{\rho_j(\omega')}{\omega' - \omega}. \quad (\text{S47b})$$

At resonance, the density of states becomes of the Lorentzian form:

$$\rho_j(\omega) = \frac{1}{\pi\hbar} \frac{\Gamma_j/2}{\omega^2 + (\Gamma_j/2)^2}. \quad (\text{S48})$$

The admittance at resonance can be simplified into

$$g(\omega) = \frac{\hbar\omega}{R_Q} \left[i\mathcal{P} \int \int \frac{d\epsilon' d\epsilon''}{\epsilon'' - \epsilon'} (f(\epsilon' - \hbar\omega) - f(\epsilon'')) \rho_1(\omega - \omega') \rho_2(\omega'') + \pi \int d\epsilon' (f(\epsilon' - \hbar\omega) - f(\epsilon')) \rho_1(\omega - \omega') \rho_2(\omega') \right] \quad (\text{S49})$$

with $\epsilon' = \hbar\omega'$ and $\epsilon'' = \hbar\omega''$ and \mathcal{P} meaning the principal value. At zero temperature, it is further simplified into

$$g(\omega) = \frac{\hbar\omega}{R_Q} \left[\pi \int_0^{\hbar\omega} d\epsilon' \rho_1(\omega - \omega') \rho_2(\omega') + i\mathcal{P} \int_{-\infty}^0 d\epsilon' \int_0^{\infty} d\epsilon'' \frac{2(\epsilon'' - \epsilon')}{(\epsilon'' - \epsilon')^2 - (\hbar\omega)^2} \rho_1(\omega') \rho_2(\omega'') \right], \quad (\text{S50})$$

justifying Eq. (12) in the main text.

Relaxation Resistance at Finite Temperatures: Sommerfeld Expansion

It is difficult to obtain an analytical expression for finite-temperature resistance. However, the low-temperature behavior can be examined by using the Sommerfeld expansion, which expands the integral as

$$\int d\epsilon f(\epsilon) h(\epsilon) = \int_{-\infty}^0 d\epsilon h(\epsilon) + \sum_{n=1}^{\infty} \alpha_{2n} (k_B T)^{2n} h^{(2n-1)}(0), \quad (\text{S51})$$

where $\alpha_{2n} = 2\zeta(2n)(1 - 2^{1-2n})$. Then, up to the second order in $k_B T$, one obtains

$$g(\omega) \approx g(\omega)|_{T=0} - \frac{1}{R_Q} \left(\frac{k_B T}{\hbar} \right)^2 \frac{\pi^2}{6} \left[\sum_{\mu} \left(\frac{\Gamma_+}{\Gamma_+ + i\omega} + \frac{\Gamma_-^2}{\varepsilon(\varepsilon - \mu\omega)} \right) \left(\frac{1}{(\omega - i\Gamma_+/2 - \mu\varepsilon/2)^2} - \frac{1}{(i\Gamma_+/2 + \mu\varepsilon/2)^2} \right) + \frac{2\Gamma_-^2\omega}{\varepsilon(\varepsilon^2 - \omega^2)} \left(\frac{1}{(i\Gamma_+/2 + \varepsilon/2)^2} - \frac{1}{(i\Gamma_+/2 - \varepsilon/2)^2} \right) \right]. \quad (\text{S52})$$

For the Dirac fermion edge mode ($\Gamma_1 = \Gamma_2$), the zero-frequency resistance at low temperatures is then given by

$$R_0 = \frac{R_Q}{2} \left[1 + \frac{4\pi^2}{3} \left(\frac{k_B T}{\epsilon_d} \right)^2 \left(\frac{(\epsilon_d/\hbar)^2}{(\epsilon_d/\hbar)^2 + (\Gamma_+/2)^2} \right)^2 \right]. \quad (\text{S53})$$

On the other hand, in the cTSC₁ phase ($\Gamma_2 = 0$), the Sommerfeld expansion of R_0 is expressed as

$$R_0 = R_Q \left(\frac{k_B T}{\epsilon_d} \right)^2 \frac{4\pi^2}{3} \left(\frac{(\epsilon_d/\hbar)^2 - \Gamma_+^2}{(\epsilon_d/\hbar)^2} \right)^2 \left(1 - i \frac{\Gamma_+}{\varepsilon} \ln \frac{\Gamma_+ - i\varepsilon}{\Gamma_+ + i\varepsilon} \right)^{-2}. \quad (\text{S54})$$

Note that the stark contrast between two cases at the resonance ($\epsilon_d = 0$): In the QAH phase the second-order term vanishes, indicating some immunity to thermal fluctuations, while R_0 diverges in the cTSC₁ phase. Surely the above expansion for the case of a single Majorana fermion edge mode is valid only for $k_B T \ll \hbar \Gamma_m$ so the $\epsilon_d \rightarrow 0$ limit cannot be taken from it. But still the non-monotonic behavior or the increase of the resistance at finite temperatures, discussed in the main text, are qualitatively captured in this expansion. In the case of weak-coupling limit ($|\epsilon_d/\hbar| \gg \Gamma_1$), the expansion leads to Eq. (13).
